An official publication of the International Society for Energy, Environment and Sustainability (ISEES)

Journal of Energy and Environmental Sustainability

Journal homepage : www.jees.in

Measurement of Drag Coefficient for an Elliptical Cylinder

P Sooraj, Amit Agrawal*, Atul Sharma

Department of Mechanical Engineering, Indian Institute of Technology Bombay, Powai, Mumbai 400 0076, India

ARTICLE INFO

Received : 30 August 2017
Revised : 27 December 2017
Accepted : 23 January 2018

Keywords:
PIV, Drag coefficient, Modified Wake Survey Method

ABSTRACT

This paper reports drag coefficient for an elliptic cylinder as obtained from PIV measurements. We first evaluate three different methods to obtain drag force on an object immersed in a flow using particle image velocimetry (PIV) data, but no additional input data. The need for such a study is felt because PIV does not directly yield pressure-field required in the calculation of drag. The methods are benchmarked against circular cylinder. The three methods yield the values of drag coefficient within 1%. The method is further applied to elliptic cylinder over a large range of Reynolds number (Re = 240 – 34,000). The value for drag coefficient for elliptic cylinder over this range is not readily available. A sensitivity analysis of the result on the size of the observation window is also provided; the results indicate that reliable results are obtained if the viewframe is located at least 2.7 C downstream and 1.1 C on either lateral side of the cylinder. The methods evaluated here can be further employed with PIV data for various flow problems.

1. Introduction

The drag on a bluff body immersed in the flow is of significant practical interest. Knowing the value of drag force is important, for example, in calculating the power requirement of airplane, submarine, etc. The use of particle image velocimetry (PIV) to obtain the velocity field has become rather standard worldwide. However, it is difficult to obtain the lift/drag forces from PIV data alone, rather additional equipment (such as load cell) is required to obtain information about the forces acting on a surface/body. This is because pressure component of drag is a substantial portion of the overall drag (up to 90% for bluff bodies), whereas pressure cannot be obtained in a direct manner from PIV. It would undoubtedly be useful to obtain force measurements from PIV data in addition to velocity (and vorticity) information. In this work, we show that mean drag force can be extracted in a reliable manner from two-dimensional PIV data using the wake survey method.

Van Oudheusden et al. (2007) estimated the force coefficient for compressible and incompressible flows using control volume approach in which they have solved pressure field using flow constitutive equations for uncorrelated PIV measurements. Kurtulus et al. (2007) calculated the force coefficient by integrating the force equations within a control volume for square cylinder using Time Resolved-PIV. Berton et al. (2004) determined the airload components acting on a blade section of a helicopter rotor in forward flight by calculating different terms in the momentum and Bernoulli equations. Koochesfahani (1989), Spedding et al. (2003, 2008), and Bohl and Koochesfahani (2009) proposed integral momentum theorem based methods for drag calculation. In their methods, the mean streamwise velocity data is applied on a control volume to estimate the mean forces. Since the pressure field is unknown, accurate calculation of the force coefficient remains elusive. Streitlien and Triantafyllu (1998) suggested that the wake survey method overestimates the thrust force for an inviscid Karman vortex street model of a wake; this is because of not considering the pressure deficit. The control volume is typically close to the body making the contribution of pressure, and therefore the overall error, relatively large.

Bohl and Koochesfahani (2009) proposed a new formulation to calculate the mean drag force where they considered all the relevant factors that affect drag force. The cross stream momentum equation is utilized in an indigenous manner in their approach. Dabiri et al. (2014) proposed an alternate method whereby the pressure-field is estimated from the PIV data by solving the Navier-Stokes equations. The pressure gradient is calculated from a time-series of velocity fields for unsteady calculations, whereas a single velocity field suffices for quasi-steady calculations. The calculation of the corresponding pressure field is made robust by determining its value along several different integration paths. Using median polling of many integration paths, the measurement errors which get accumulated along each integration path can be reduced, allowing accurate determination of the pressure field and its gradient. Once the pressure-field is known, the drag force is calculated by integrating the pressure around the surface of the body.

The purpose of this investigation is two-fold: first, to evaluate various methods for obtaining the drag coefficient; second, to apply the

* Corresponding Author: *amit.agrawal@iitb.ac.in*

methods to obtain drag coefficient for an elliptic cylinder over a wide range of Reynolds number. Accordingly, based on the approaches of Bohl and Koochesfahani (2009) and Dabiri et al. (2014), we propose and compare three variants of their methods to calculate the mean drag force on an object from PIV data, without any additional input data. We also perform a sensitivity analysis of the result on the size of the observation window. One method is based on modified wake survey method, whereby only velocity data is used. In the other two methods both velocity and pressure data is used in the calculations. All the three methods are tested on flow over an elliptical cylinder (243 < Re < 33,790). The range of Reynolds number covered here is relevant for heat exchangers (Ota et al. 1984). The present data can also be utilized for benchmarking numerical results, and for understanding differences between circular and elliptic cylinders. Ota et al. (1986) noted that elliptical cylinders can be used for high performance heat exchanger in order to save energy; and recommend elliptic cylinders over circular cylinder. We show that all the three methods yield approximately the same value of drag coefficient. We further show that our value of drag coefficient for a circular cylinder (120 <Re < 17,000) compares well with the literature value, suggesting that these variants are also accurate.

2. Materials and Methods

The PIV experiments were conducted in a closed-loop water tunnel (Fig. 1a) with a working section of 400 × 400 mm^2 cross-section and a length of 1500 mm (Fig. 1b). The models (circular and elliptical cylinders) employed were made of acrylic. Acrylic being transparent allows imaging on both sides of the cylinder, other than a narrow shadow-region at the edges of the cylinder. The circular cylinder has a diameter of 10 mm and a length of 150 mm. The Reynolds number for circular cylinder is in the range of 120 to 17,000. The elliptical cylinder has a major axis of 40 mm and a minor axis of 20 mm. The length of the cylinder is 300 mm. The blockage ratio for the present measurements is therefore less than 5%. The flow velocity ranges from 11 to 1520 mm/s. The Reynolds number for elliptical cylinder ranges from 243 to 33,790. The minor axis of the elliptical cylinder is used as the characteristic length while free-stream velocity is used as the characteristic velocity scale for Reynolds number calculation.

Schematic diagram of the PIV setup is given in Fig 1(c). The seed particles are made of glass with diameter in the range of 8-10m. The particles are illuminated by dual Nd-YAG lasers (Beamtech, China;

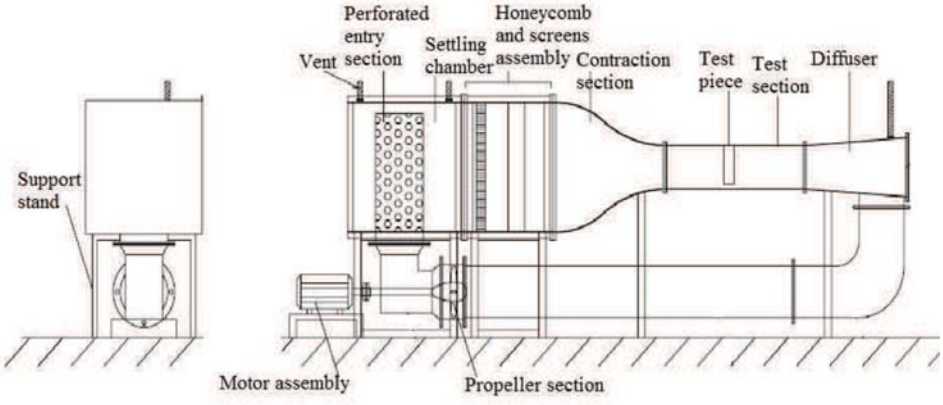

Figure 1: Schematic Representaion of (a) Water tunnel facility (b) Elliptic cylinder employed in measurements. (c) PIV set up.

wavelength 532 nm, energy: 200 mJ/pulse, repetition rate: 15Hz) and a CCD camera (PCOPixefly, Germany; image size: 1392 x 1024 pixels) is used to capture the images which are later analysed using a PIV software (Sewatkar et al. 2012; Hashiehbaf et al. 2015). It was verified that the Stokes criteria is satisfied, as the value of Stokes number (St) is of the order of 10^{-4} to 10^{-6}. Since the value is much smaller than 0.1, particles trace the fluid motion closely with an error of less than 1% (Pescini et al., 2015). The successive image pairs are captured at 5 Hz. The time delay between a pair of PIV images is between 1-60 ms, depending on the speed of the flow. The interrogation window size used for cross correlation were 32×32 pixels with 50% overlap. The velocity vectors are obtained using the cross correlation method. The average velocity, υ_{avg} is calculated by taking the mean velocity over 150 frames. Convergence test confirmed that the number of frames is adequate for calculating the flow statistics.

2.1 Wake survey method (using velocity field)

In this method (Bohl and Koochesfahani 2009), the average pressure $p_{avg}(y)$ needed at the downstream control surface (BC; Fig. 2) is obtained from the mean cross stream momentum equation. Neglecting the mean transverse velocity v_{avg} and streamwise gradient of Reynolds stress, the mean cross stream momentum equation gets simplified as:

$$\frac{\partial p_{avg}}{\partial y} = -\rho \frac{\partial v_{rms}^2}{\partial y} \tag{1}$$

Note that the free stream speed u_o at the downstream location (i.e. at sufficient lateral distance away from the body) is slightly different from the upstream speed u_∞ (Fig. 2). Similarly, the corresponding free stream pressure p_o is slightly different from the upstream pressure p_∞ because the integration domain H is typically not large enough. Knowing u_∞, u_o and p_∞, can be calculated using the Bernoulli equation (the use of this equation can be easily justified because the flow is essentially irrotational, and therefore inviscid, laterally away from the body):

$$p_0 = p_\infty + {}^1\!/_2\, \rho(u_\infty^2 - u_0^2) \tag{2}$$

The above simplified cross stream momentum equation (Eq. 1) was integrated using the free stream pressure p_o and realizing that the corresponding V_{rms} is zero (i.e. in the free stream region). Therefore the downstream average pressure distribution was obtained as:

$$p_{avg}(y) = -\rho v_{rms}^2(y) + p_0 \tag{3}$$

Substitute p_o from (Eq. 2) to (Eq.3), we obtain

$$p_{avg}(y) = p_\infty + \frac{1}{2}\rho(U_\infty^2 - U_0^2) - \rho v_{rms}^2(y) \tag{4}$$

Note that the streamwise component of the momentum flux through the lateral control surface also affects the force on the control volume. This becomes all the more relevant when H is not taken far away from the body. The velocity along the control surface varies between u_∞ and u_0. Again following Bohl and Koochesfahani (2009), the average of these velocities is taken as the effective velocity and represented as $(1 - \varepsilon)\, u_\infty$ (where ε is supposed to be sufficiently smaller than unity)

Finally, the average drag force was calculated using the streamwise momentum equation. Note that in this formulation, the contributions of fluctuating velocity and pressure terms are suitably accounted for. The contributions of fluctuating velocity and pressure terms are indeed substantial if the control volume is not chosen sufficiently far away from the body. Therefore, we can write for the coefficient of drag (Bohl and Koochesfahani 2009):

$$C_D = \frac{2}{C}\int_{-H}^{+H}\left(\frac{u_{avg}}{u_\infty}\left(\frac{u_{avg}}{u_\infty} - 1\right) + \varepsilon\left(\frac{u_{avg}}{u_\infty} - 1\right) + \left(\frac{u_{rms}}{u_\infty}\right)^2 - \left(\frac{v_{rms}}{u_\infty}\right)^2 + \frac{1}{2}\left(1 - \frac{u_0^2}{u_\infty^2}\right)\right)dy \tag{5}$$

where the integration is over the edge BC. The contribution of various terms for flow around an elliptic cylinder in the above equation have been analyzed and presented later in Fig. 5a.

2.2 Surface force based method

In this method, the instantaneous drag force is calculated by integrating pressure and shear forces around the surface of the body (Kundu and Cohen, 2004). Queen 2.0 software (refer Dabiri et al. 2014) is used to calculate the instantaneous pressure field from the instantaneous PIV data. Queen software is a Matlab based software package which takes 2D or 3D velocity field data as input; in addition, the coordinates of a solid object in the flow can be specified. The software then computes the corresponding pressure field; it can also compute unsteady pressure due to accelerating flows, added mass/acceleration reaction in flow-structure interactions with moving and deformable bodies. The shear stress on the surface of the body was calculated directly from the PIV data. The calculation of velocity gradient however needs to be performed with care, as the body may not be well aligned with the PIV grid. Queen's software solves the Navier-Stokes equation to obtain the pressure gradient from time series of velocity fields for unsteady flows and from a single velocity field for quasi-steady problems. They had used median polling of several integration paths so as to obtain the pressure gradient with minimum error.

Therefore, the net force acting on the body was calculated as:

$$F_D = \int (-p\boldsymbol{nn} + \boldsymbol{\tau}).\boldsymbol{n}_\infty d\boldsymbol{S} \tag{6}$$

where p is pressure, τ is shear stress acting on the surface of the body, n is vector unit normal to the surface, n_∞ is unit vector in the direction of upstream flow, dS is infinitesimal surface element of area, and integration is performed over the entire surface of the cylinder. The obtained force is non-dimensionalized using free stream velocity (u_∞) and minor axis (C) as the characteristic velocity and length scale respectively, to obtain the drag coefficient.

2.3 Modified wake survey method (using velocity and pressure fields)

In this method, a modified form of the wake survey method is employed to calculate the mean drag coefficient. Since the control surface is not

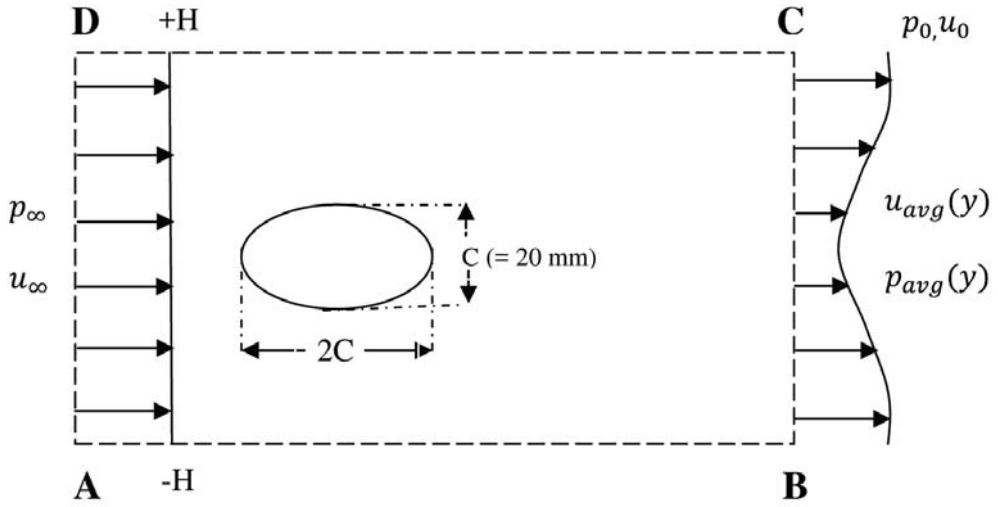

Figure 2: Control volume employed to evaluate the drag coefficient using Method 1.

taken far away from the body, the static pressure will not be the same at upstream and downstream profiles; the upstream and downstream pressures were taken from the Queen's software. The momentum balance was done using the traditional momentum integral theorem as:

$$C_D = \frac{2}{C}\int_{-H}^{+H}\left(\frac{u_{avg}}{u_\infty}\left(\frac{u_{avg}}{u_\infty}-1\right)+\varepsilon\left(\frac{u_{avg}}{u_\infty}-1\right)\right)dy + \frac{1}{2\rho u_\infty^2 C}\int_{-H}^{+H}(p_{in}-p_{out})\,dy \quad (7)$$

where p_{in} and p_{out} are the average inlet and outlet pressures respectively.

2.4 Uncertainty Estimation in the various Methods

It is difficult to estimate the uncertainty in each of the above methods without detailed modeling; however, an attempt is made to provide meaningful estimate of the uncertainty value in this section.

For estimating the uncertainty in mean velocity, we have considered all the four main factors which are responsible for uncertainty with PIV measurements. As explained in Raffel et al. (1998), Wang et al. (2008) and Lazar et al. (2010), these factors are uncertainty related to equipment, uncertainty in particle lag, sampling, and image processing. After estimating the individual uncertainty in each of these factors, the uncertainties were combined using the standard uncertainty propagation method (Yadav et al. 2015). The maximum uncertainty in mean velocity is estimated as 2.8%. Similarly, the uncertainty in velocity r.m.s. (root mean square) was estimated (as per the above references). The maximum values of uncertainty in u_{rms} and v_{rms} are 3.2% and 3.3% respectively.

The calculation of pressure is required in Methods 2 and 3; the value of pressure was calculated using the Navier-Stokes equations with velocity field as the input. As suggested by Moffat (1988), the uncertainty in calculation of pressure requires that the velocity of each point was perturbed individually over its uncertainty interval, and then fed into the Navier-Stokes equations for calculation of pressure. The resulting uncertainties in pressure was combined using the uncertainty propagation method. This was rather cumbersome and has not been attempted here. Here, the Bernoulli equation has been employed to estimate the uncertainty in pressure knowing the uncertainty in velocity. Similarly, uncertainty in shear stress (required in Method 2) is estimated from the mean velocity gradient.

The uncertainty in drag coefficient from the three methods was obtained by combining the uncertainty in individual parameters (in Eqs. 5, 6, 7 respectively) using the uncertainty propagation method. The uncertainty in drag coefficient is expected to be smaller than that calculated above because of the process of integration. The final uncertainty values in drag coefficient from each of the three methods were found to be 5.2%, 4.6% and 9.0% respectively.

3. Results and Discussion

3.1 Drag coefficient for elliptical cylinder

All the three methods were used to calculate the drag coefficient for flow around an elliptical cylinder at different Reynolds numbers. Flow field around an elliptic cylinder is shown through Figure 3. The origin of the coordinate system was fixed at the rear stagnation point of the cylinder, and distances (x and y) have been normalized (X = x/C; Y = y/C). The vector field resolution is about 1 vector per 1.5 mm. The quality of data was observed to be good other than in the shadow region located below the edges of the cylinder. The percentage of rejected vectors is below 5% for all cases. The control surfaces employed in the analysis is apparent from the figure. Note that the control surfaces are reasonably close to the body (upstream surface about 0.1 chord length; lateral surfaces: about 1 C and 2 C; and downstream surface about 3 C, away from the surface of the cylinder). Our preliminary sensitivity analysis suggested that the same values of drag coefficient are obtained by choosing control surfaces slightly inside the measured frame.

The sensitivity analysis results for different positions of the control surface for Method 1 is presented in Fig. 4. The drag coefficient values for various downstream distances are calculated and shown in Fig. 4a, for three values of Reynolds numbers covering the entire range of Re investigated here. The others control surfaces were taken at the edge of the viewframe for this test. The value was found to change by less than 6% by moving the control surface from 2.7 C to 3 C distance from the rear edge of the cylinder. Similarly, the position of the lateral surfaces was changed from 0.55 C to 1.4 C, while keeping the upstream and

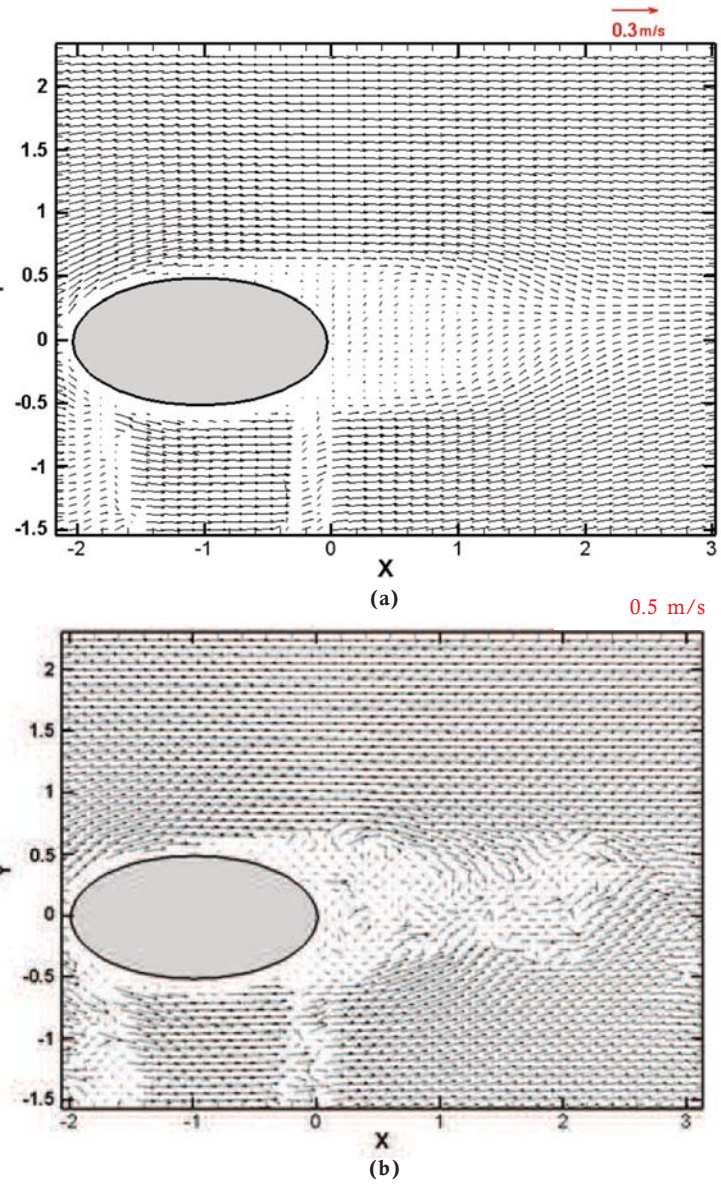

Figure 3: (a) Time averaged PIV image of flow around elliptical cylinder at Re = 2818. (b) Instantaneous velocity vector image at Re = 4919.

downstream control surfaces at the edges of the viewframe. Again, satisfactory convergence is shown by the results presented in Fig. 4b. Additional tests where all the location of all control surfaces was simultaneously changed were also undertaken (results not presented).

The value of drag coefficient as obtained from the three methods is compared in Figure 5a. All the methods are giving almost equal values for a particular Reynolds number. The difference between these methods is noted to be less than 1% over more than two decades of Reynolds number. Notice that the value of mean drag coefficient decreases from 1.5 to 0.5 with increase in Reynolds number over the range investigated. Data for the present range of Reynolds number does not seem to be readily available. For example, the data by Sivakumar et al. (2007) is for Re < 40; that by Lindsey (1938) is for Re > 60,000. Terukazu et al. (1983) studied the heat transfer characteristics and plotted the pressure coefficient around the body for Re = 8000 to 79,000; however, results for drag coefficient were not presented. Patel (1980) and Faruquee et al. (2007) studied the flow dynamics numerically for Re = 200 and 40 respectively. The data of Modi et al. (1992) is between Re = 30,000 to 10^5. Nair and Sengupta (1997) numerically analyzed the flow around an elliptical cylinder at Re = 3000 and 10,000. The present measurements assume further significance in view of absence of reliable data for drag coefficient of elliptical cylinder.

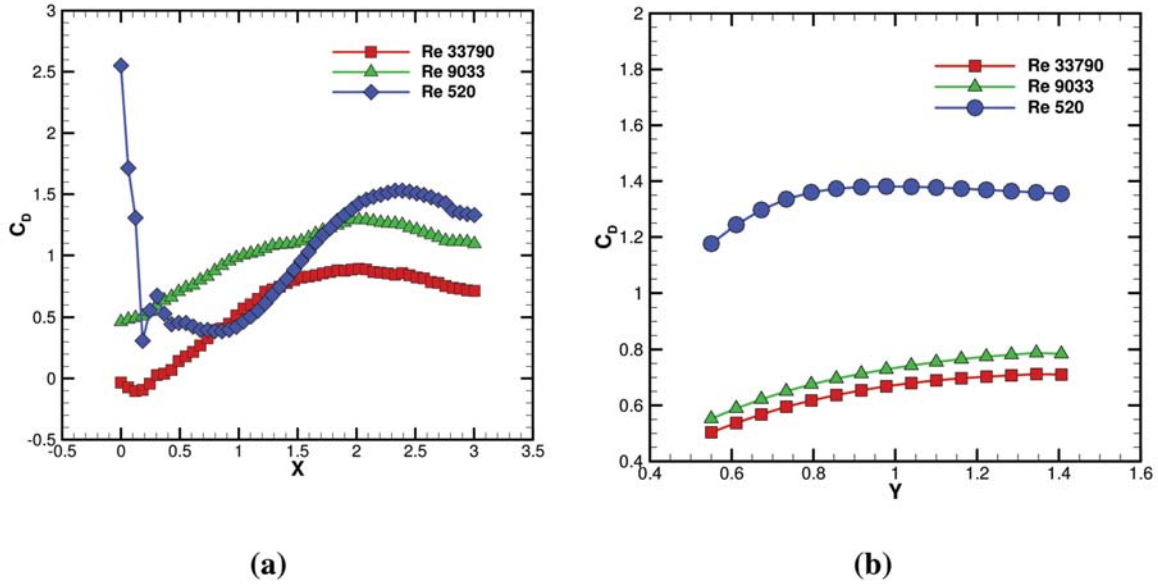

Figure 4: Drag coefficient at (a) Different downstream positions for different Reynolds number, (b) Downstream distance of 2.7 C for different lateral distances.

Khan et al. (2005) calculated the drag coefficients analytically for a wide range of Reynolds number. The present results are compared against their analytical results in Fig. 5a. Note that the results of Khan et al. (2005) are modified because of difference in characteristic length scale employed in the two works – minor axis considered here as opposed to major axis in their work. Although the trend is same, there is substantial difference in the values, with the difference increasing from 5.1% at Re = 243 to 66% at the highest value of Reynolds number (Re = 33,790). This increase in difference with Re is probably because the theoretical analysis employed by Khan et al. becomes less accurate at higher Reynolds numbers. Khan et al. while comparing their theoretical results for circular cylinder with the experimental results of Wieselsberger (1921) also noted a similar qualitative agreement only with the experimental values; although the agreement with the experimental data was much better at higher Reynolds number in that case.

The average coefficient of pressure around the top surface of the elliptic cylinder as determined using the average velocity field is plotted in Fig. 5b for three different values of Reynolds numbers. The pressure variation was qualitatively similar to that of a circular cylinder. The pressure coefficient was maximum at the front stagnation point and reduces because of acceleration of the flow. The minimum value of pressure coefficient was seen at the top surface, beyond which it starts to recover. However, the recovery was truncated owing to flow separation on the rear-half of the cylinder.

The results in this section show that the three methods yield approximately the same value of drag coefficient. Further, the value of drag coefficient for an elliptic cylinder is reported for the Reynolds number range, which seems to be missing from the literature.

3.2 Drag coefficient for circular cylinder

The methods described in Section 2 are also used to estimate the drag coefficient around a circular cylinder and the results are presented in Fig. 6a. Due to limitation in the image quality, it was not possible to extract pressure on the cylinder surface; therefore, results from Method 2 are not

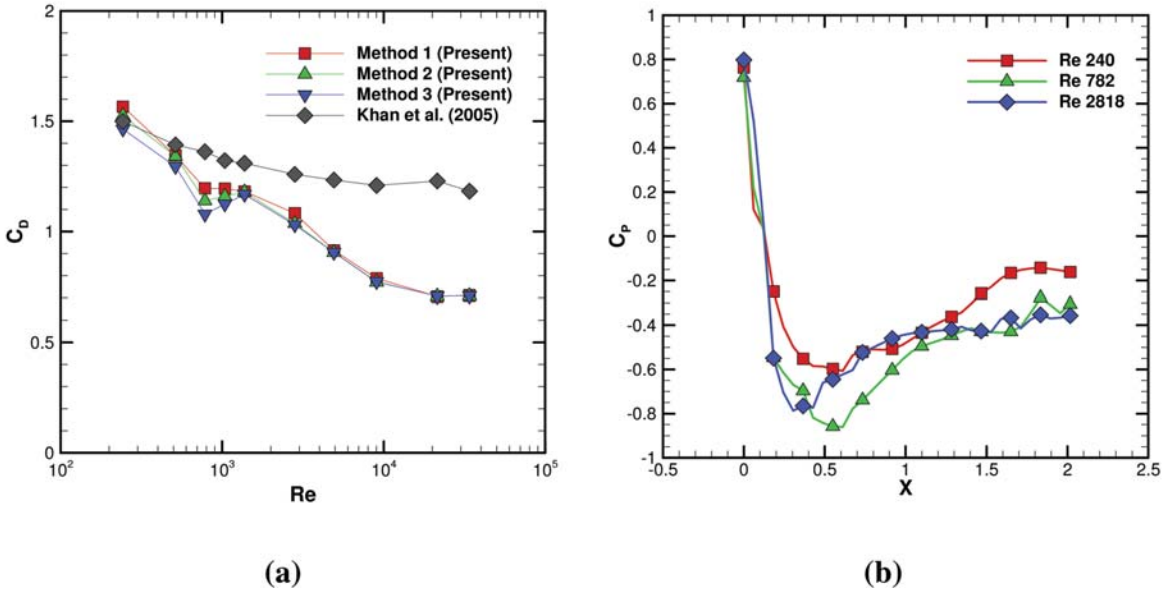

Figure 5: (a) Drag coefficient versus Reynolds number for an elliptical cylinder as obtained from the three methods, the analytical result of Khan et al. (2005) is also included for comparison. (b) Coefficient of pressure around the elliptical cylinder at different Reynolds numbers.

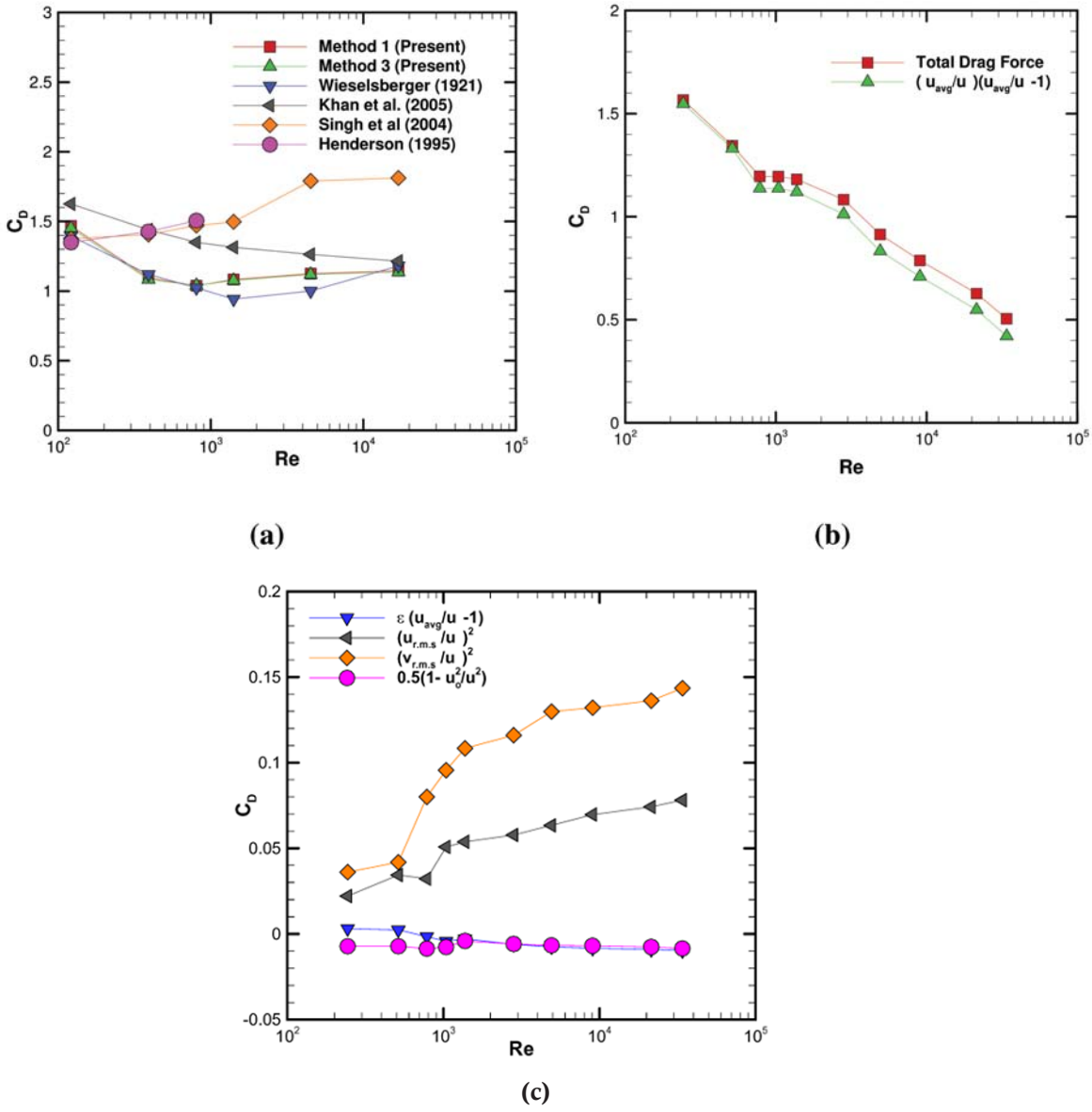

Figure 6: (a) Drag coefficient versus Reynolds number for a circular cylinder, and comparison with reported values. The experimental data from Wieselsberger (1921) is taken from Roshko (1961). (b - c) Components of Drag coefficient (Method 1) versus Reynolds number for an elliptical cylinder.

being presented here. The obtained results are compared against the experimental results of Wieselsberger (1921), numerical results of Singh et al. (2004) and Henderson (1995); and theoretical results of Khan et al. (2005).The overall agreement of the above results is reasonable. In particular, the deviation with respect to that of Wieselsberger (1921) is within 2.5 to 15%. These measurements show that the methods employed here yield the value of drag coefficient accurately.

The drag force values are typically measured using force sensors, while PIV is employed to obtain the flow field. The two equipments together help understand the flow physics better. Our first contribution here is to eliminate the need for having an additional force sensor; rather we rely only on the PIV technique to uncover both the flow field as well as force information (at least to a limited extent).

Note that only wholefield velocity information is required in Method 1 (i.e., calculation of pressure is not explicitly required in this method), whereas the other two methods require calculation of pressure. Calculation of r.m.s. of both velocity components is however required in Method 1. When the control volume is close to the bluff body, pressure deficit occurs between the inlet and outlet of the control volume which is accounted for by the velocity fluctuation terms in Method 1.

The contribution of the individual terms in Method 1 has been analyzed for elliptical cylinder as a function of Reynolds number; see Figure 6b. It is interesting to note that the contribution of the first term of Eq. 5 is more than 99% at lower Reynolds number, and reduces to 83.6% at the highest Reynolds number. The contribution of the second and fifth terms in Eq. 5 is seen to be small over the entire range of Reynolds number. For example, $u_{o/u\infty}$ varies between 1.03 to 1.05 for different Reynolds number and ϵ varies from -0.0369 to -0.0162 over the same range. The contribution of velocity r.m.s. is (understandably) negligibly small at low Reynolds number, but becomes up to 16% at higher values of Re. Notice that the value of v_{rms} is about 83% higher than the value of thereby leading to a higher contribution of the former in the overall value of drag coefficient. The result also suggests that the flow is highly anisotropic close to the cylinder.

Notice that the drag coefficient is obtained using the mean value of velocity and pressure in Methods 1 and 3; whereas instantaneous values are employed in Method 2. The mean drag coefficient can subsequently be obtained by time averaging the instantaneous drag coefficient values in method 2. Methods 1 and 3 are applied at the edges of the control volume (which are regular geometric surfaces) and therefore easier to apply than Method 2 (requiring calculation on the body surface). This advantage becomes particularly pronounced if the body is of irregular shape, or if the body is moving.

4. Conclusions

Results suggest that all the three methods tested here gave the same value of drag coefficient and therefore any one of them could be employed based on the type and quality of data available from PIV measurements. However, modified wake survey method yielded higher uncertainty, at least for the conditions tested here, as compared to the other two methods. A quantitative comparison of the result obtained presented above should enhance confidence on their method. This study has provided value of mean drag coefficient for elliptical cylinder over a wide range of Reynolds number ($243 < Re < 33{,}790$); such data was missing from the literature. This data could potentially be useful for benchmarking numerical analysis and for understanding flow in heat exchangers involving elliptic tubes.

Acknowledgement

We are grateful to Naval Research Board, New Delhi for funding the water tunnel facility employed in the measurements.

References:

[1]. Bohl D G and Koochesfahani M M, 2009, MTV measurements of the vortical field in the wake of an airfoil oscillating at high reduced frequency, Journal of Fluid Mechanics, 620, 63-88.

[2]. Berton E, Maresca C and Favier D, 2004, A new experimental method for determining local airloads on rotor blades in forward flight, Exp. Fluids, 37, 455–457

[3]. Dabiri JO, Bose S, Gemmell BJ, Colin S P and Costello J H, 2014, An algorithm to estimate unsteady and quasi-steady pressure fields from velocity field measurements, *Journal of Experimental Biology*, 217, 331-336.

[4]. Faruquee Z, Ting D S, Fartaj A, Barron R M and Carriveau R, 2007, The effects of axis ratio on laminar fluid flow around an elliptical cylinder, International Journal of Heat and Fluid Flow, 28(5), 1178-1189.

[5]. Hashiehbaf A, Baramade A, Agrawal A and Romano G P, 2015, Experimental investigation on an axisymmetric turbulent jet impinging on a concave surface, International Journal of Heat and Fluid Flow, 53, 167-182.

[6]. Henderson R D, 1995, Details of the drag curve near the onset of vortex shedding, Physics of Fluids (1994-present), 7(9), 2102-2104.

[7]. Khan W A, Culham R J and Yovanovich M M, 2005, Fluid flow around and heat transfer from elliptical cylinders: analytical approach, Journal of Thermophysics and Heat Transfer, 19(2), 178-185.

[8]. Koochesfahani M M, 1989, Vortical patterns in the wake of an oscillating airfoil, AIAA J, 27, 1200.

[9]. Kundu P K and Cohen IM, 2004, Fluid mechanics, Elsevier Academic Press, San Diego, 2008.

[10]. Kurtulus D F, Scarano F and David L, 2007, Unsteady aerodynamic forces estimation on a square cylinder by TR-PIV, Experiments in Fluids, 42 (2), 185-196.

[11]. Lazar E, DeBlauw B, Glumac N, Dutton C, and Eliott G, 2010, A Practical Approach to PIV Uncertainty Analysis, 27th AIAA Aerodynamics Measurement Technology and Ground Testing Conference, 493.

[12]. Lindsey W F, 1938, Drag of cylinders of simple shapes, Report no. 619, National Advisory Committee for Aeronautics.

[13]. Modi V J, Wilandt E, Dikshit AK and Yokomizo T, 1992, On the fluid dynamics of elliptic cylinders, The Second International Offshore and Polar Engineering Conference, 14-19 June, San Francisco, California, USA.

[14]. Moffat R J, 1988, Describing the uncertainties in experimental results, Experimental thermal and fluid science, 1(1), 3-17.

[15]. Nair M T and Sengupta T K, 1997, Unsteady flow past elliptic cylinders, Journal of Fluids and Structures, 11(6), 555-595.

[16]. Ota T, Nishiyama H, and Taoka, 1984, Heat Transfer and Flow around an Elliptic Cylinder, Int. J. Heat Mass Transfer, 27, 1771-1779.

[17]. Ota T, Nishiyama H, Kominami J and Sato K, 1986, Heat Transfer from Two Elliptic Cylinders in Tandem Arrangement, ASME Journal of Heat Transfer, 108, 525-531.

[18]. Patel V A, 1981, Flow around the impulsively started elliptic cylinder at various angles of attack, Computers and Fluids, 9(4), 435-462.

[19]. Pescini E, Francioso L, De Giorgi M G and Ficarella A, 2015, Investigation of a Micro Dielectric Barrier Discharge Plasma Actuator for Regional Aircraft Active Flow Control, Plasma Science, IEEE Transactions on, 43(10), 3668-80.

[20]. Raffel M, Willert C, and Kompenhans J 1998 Particle Image Velocimetry: A Practical Guide, Springer-Verlag, Berlin.

[21]. Roshko A, 1961, Experiments on the flow past a circular cylinder at very high Reynolds number, Journal of Fluid Mechanics, 10(3), 345-356.

[22]. Sewatkar C M, Patel R, Sharma A and Agrawal A, 2012, Flow around six in-line square cylinders, Journal of Fluid Mechanics, 710, 195-233.

[23]. Singh S P and S Mittal, 2005, Flow past a cylinder: shear layer instability and drag crisis, International Journal for Numerical Methods in Fluids, 47(1), 75-98.

[24]. Sivakumar P, Bharti R P and Chhabra R P, 2007, Steady flow of power-law fluids across an unconfined elliptical cylinder, Chemical Engineering Science, 62(6), 1682-1702.

[25]. Spedding G R, Hedenstrom A and Rosen M, 2003, Quantitative studies of the wakes of freely flying birds in a low-turbulence wind tunnel, Exp Fluids, 34, 291.

[26]. Spedding G R and Hedenstrom A, 2009, PIV-based investigations of animal flight, Exp Fluids, 46(5), 749-763.

[27]. Streitlien K and Triantafyllou G S, 1998, On thrust estimates for flapping airfoils, J. Fluids Struct., 12, 47.

[28]. Terukazu O, Hideya N and Yukiyasu T, 1984, Heat transfer and flow around an elliptic cylinder, International Journal of Heat and Mass Transfer, 27(10), 1771-1779.

[29]. vanOudheusden B W,Scarano F, Roosenboom E W M, Casimiri E W F and Souverein L J, 2007, Evaluation of integral forces and pressure fields from planar velocimetry data for incompressible and compressible flows, Experiments in Fluids, 43(2-3), 153-162.

[30]. Wang L, Hejcik, J and Sunden B, 2007, PIV Measurement of Separated Flow in a Square Channel With Streamwise Periodic Ribs on One Wall, ASME J. Fluids Eng., 129(7), 834–841.

[31]. Wieselsberger C, 1921, Neuero Feststellungen über die Gesetze des Flüssigkeits- und Luftwiderstands, Phys. Z., 22, 321–8

[32]. Yadav H, Srivastava A and Agrawal A, 2015, Characterization of Pulsating Submerged Jet-A PIV Study, Journal of Thermal Science and Engineering Applications, 8(1), 011014.